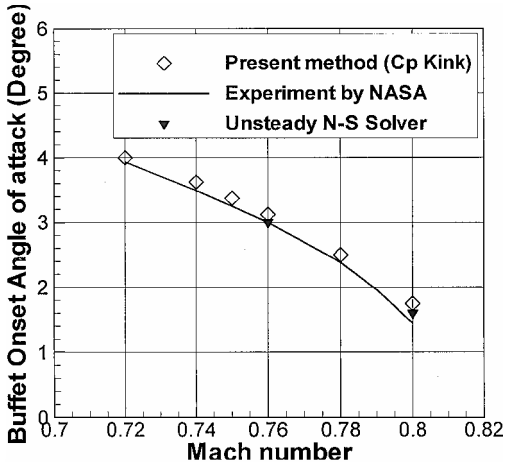

Fig. 3 Comparison of buffet onset, $Re = 6.0 \times 10^6$.

oscillations are small enough so that steady state may be assumed to estimate the mean value.

As an alternative method, a frequently used method is analysis of pitching moment curve deviation[6] as shown in Fig. 2b. The pitching moment is referenced at the leading edge. Figure 2b shows more obvious slope changes in the curves than those in the lift curves. The variation of pitching moment is sensitive due to the length between the reference point and the point in the separated region. As the separated region moves aft with movement of the shock, this effect is accentuated.

The movement of the shock wave with variation in angle of attack causes changes in the position of the center of pressure. Note that the center of pressure curves show noticeable kinks, as shown in Fig. 2c, compared with other curves. This occurs because the effect of shock movement causes a relatively small variation of lift in general, but it causes drastic variation on position of center of pressure. Furthermore, this effect is accentuated when shock-induced separation exists. These kink points coincided with those in the lift curves and pitching moment curves, as shown in Figs. 2a–2c. Therefore, the kink points in the center of pressure curves can be recognized as buffet onset points.

The predicted results of transonic buffet onset for the NACA 0012 airfoil are shown in Fig. 3 along with those of two-dimensional buffet wind-tunnel test.[10] Figure 3 shows that the predicted results of the present method are very close to the experimental predictions, except for results at the higher mach number. These discrepancies at higher Mach number are due to the difference between the shock locations predicted by experiments and computations. A more advanced turbulence model may alleviate this problem. Unsteady prediction is carried out for the cases of Mach numbers 0.76 and 0.80. Buffet onset is predicted almost exactly as shown in Fig. 3. However, this prediction requires very long computing time and large memory.

Conclusions

The new theoretical steady approaching method developed is useful to predict the buffet onset for an airfoil with shock-induced separation bubble (model A airfoil) when compared with the two-dimensional buffet wind-tunnel test. Among the various aerodynamic curves, the center of pressure curve shows the most distinct kink point even at relatively low Mach number with high angle of attack and good agreement with unsteady wind-tunnel test results. Therefore, it can be suggested that the kink of the center of pressure vs angle-of-attack curve can be used as a reliable indicator of buffet onset on a model A airfoil for the steady experimental method. In addition, in comparison with the results of unsteady prediction method, which requires more computational time and memory, the present method is shown to be accurate for transonic buffet onset prediction from the engineering application viewpoint. Because the present method applies the kink analysis method to curves calculated from steady Navier–Stokes solver, it can be applicable even to the three-dimensional full configuration of aircraft.

References

[1]Thomas, F., and Redeker, G., "A Method for Calculating the Turbulence Buffet Boundary Including the Influence of Reynolds Number," CP-83, AGARD, 1971.

[2]Pearcey, H. H., Osborne, J., and Haines, A. B., "The Interaction Between Local Effects at the Shock and Rear Separation—A Source of Significant Scale Effects in Wind-Tunnel Tests on Airfoils and Wings," CP-35, AGARD, 1968.

[3]Thomas, F., "The Determination of the Buffet Boundaries of Aerofoils in the Transonic Regimes," Aircraft Research Association, Ltd., Library Translation No. 19, Bedford, England, U.K., Feb. 1969.

[4]Redeker, G., and Proksch, H. J., "The Prediction of Buffet Onset and Light Buffet by Means of Computational Methods," CP-204, AGARD, 1977.

[5]Pearcey, H. H., and Holder, D. W., "Simple Method for the Prediction of Wing Buffeting Resulting from Bubble Type Separation," NPL Aero Rept. 1024, June 1962.

[6]Pulliam, T. H., and Chausse, D. S., "A Diagonal Form of an Implicit Approximate-Factorization Algorithm," *Journal of Computational Physics*, Vol. 39, 1981, pp. 347–363.

[7]Baldwin, B. S., and Lomax, H., "Thin Layer Approaimation and Algebraic Model for Separated Turbulent Flows," AIAA Paper 78-257, Jan. 1978.

[8]Levy, L. L., Jr., and Bailey, H. E., "Computation of Airfoil Buffet Boundaries," *AIAA Journal*, Vol. 19, No. 11, 1981, pp. 1488–1490.

[9]Holst, T. L., "Viscous Transonic Airfoil Workshop Compendium of Results," AIAA Paper 87-1460, June 1987.

[10]McDevitt, J. B., and Okuno, A. F., "Static and Dynamic Pressure Measurements on a NACA0012 Airfoil in the Ames High Reynolds Number Facility," NASA TP-2485, June 1985.

Characteristics of Compressible Concave-Corner Flows

Kung-Ming Chung*
National Cheng-Kung University, Tainan 711, Taiwan, Republic of China

Nomenclature

C_p	=	pressure coefficient, $(p_w - p_\infty)/q_\infty$
M_∞	=	freestream Mach number
p	=	static pressure
q_∞	=	dynamic pressure
x	=	coordinate along the surface of the corner
x^*	=	x/δ_0
x_u^*, x_d^*	=	normalized upstream and downstream influence region
α	=	concave-corner angle, deg
δ_0	=	incoming boundary-layer thickness
η	=	convex-corner angle, deg
ξ	=	interaction region, $(x_d^* - x_u^*)$

Introduction

IMPROVEMENT of aircraft performance is always one of the major goals for the aerodynamists.[1] Bolonki and Gilyard[2] have indicated that the deflected control surfaces could be used in combination to provide the variable camber control within the operational flight envelope. The active modification of the control surfaces could potentially play a role in performance optimization for an aircraft. At transonic speeds the benefits of variable camber using a simple trailing-edge control surface system can approach more than

Received 26 May 2002; revision received 3 April 2003; accepted for publication 3 April 2003.

*Research Fellow, Aerospace Science and Technology Research Center, 2500 Section 1, Chung-Cheng S. Rd, Kueijen. Senior Member AIAA.

10% in maximizing the lift-to-drag ratio and induce higher buffet boundary.[3] However, the critical Mach number, onset of boundary-layer separation, and drag are also strongly related to the allowable deflection of the control surfaces. A simplified model of the upper deflected control surface (or convex-corner flows) was studied by Chung.[4] It was found that the transition of expansion flows, initial boundary-layer separation, separation length, and characteristics of surface pressure fluctuations can be scaled with $M_\infty^2\,\eta$.

To characterize the aerodynamic performance of a deflected control surface, a study of the lower deflected control surface is required. The present study examined a turbulent boundary layer over concave corners at $M_\infty = 0.64$ and 0.83. This investigation involved the subsonic flows over small to larger concave corners. Measurements of surface pressure were taken to study the interaction region and characteristics of pressure distributions.

Experiment

Transonic Wind Tunnel

The ASTRC/NCKU transonic wind tunnel is blowdown type and operates in the Mach number from 0.2 to 1.4 at Reynolds numbers up to 20×10^6/m. Major components of the facility include compressors, air dryers, cooling water system, storage tanks, and the tunnel. The dew point of high-pressure air through the dryers is maintained at -40°C under normal operation conditions. Air storage volume for the three storage tanks is up to 180 m^3 at 5.15 MPa. The test section is 600 mm square and 1500 mm long. In the present study the test section was assembled with solid side walls and perforated top/bottom walls to reduce the background acoustic noise. The freestream Mach numbers were 0.64 and 0.83 ± 0.01, and the stagnation pressure p_0 and temperature T_0 were 172 ± 0.5 kPa and room temperature, respectively.

For the data-acquisition system the NEFF Instruments System 620 and the LeCroy waveform recorders were used. The test conditions were recorded by the NEFF system, whereas the LeCroy 6810 waveform recorders were used for the surface-pressure measurements. A host computer with CATALYST software controlled the setup of LeCroy waveform recorders through a LeCroy 8901A interface. All input channels were triggered simultaneously by using an input channel as the trigger source.

Test Model

The test model consisted of a flat plate and an interchangeable instrumentation plate. The test model was 150 mm wide and 600 mm long, which was supported by a single sting mounted on the bottom wall of the test section. The concave corner, with 3-, 5-, 7-, 10-, and 15-deg angles (α), was located at 500 mm from the leading edge of the flat plate. One row of 19 holes, 6 mm apart and 2.5 mm in diameter, was installed along the centerline of each instrumentation plate perpendicular to the test surface. All of the pressure transducers within the holes were flush mounted to the test surface and potted using silicone sealant. The side fences at both sides of the instrumentation plate were installed to prevent crossflow.

Experimental Techniques

For the surface-pressure measurements the Kulite pressure transducers (Model XCS-093-25A, B screen) powered by a TES Model 6102 power supply at 15.0 V were used. The outside diameter was 2.36 mm, and the sensing element was 0.97 mm in diameter. The natural frequency was 200 kHz as quoted by the manufacturer. External amplifiers (Ecreon Model E713) were used to improve the signal-to-noise ratio. The typical sampling period is 5 μs (200 kHz). Each data record possessed 131,072 data points for the statistical analysis. The data were divided into 32 blocks. The mean values of each block (4096 data points) were calculated. Variations of the blocks were estimated to be 0.43 for the mean surface-pressure coefficient C_p, which is considered to be the uncertainty of experimental data.

For the pitot-pressure survey of incoming boundary layer, the normalized velocity profiles for the undisturbed boundary layer at 25 mm upstream of the concave corner appear to be full ($n \approx 7$–11 for the velocity power law). This indicates turbulent flow at the measurement locations. The boundary-layer thickness is estimated to be 7.3 and 7.1 ± 0.2 mm for $M_\infty = 0.64$ and 0.83, respectively.

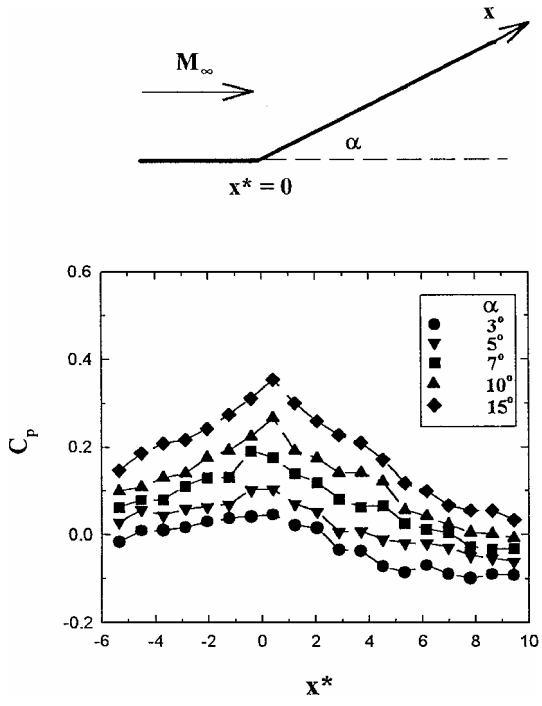

Fig. 1 Static-pressure distributions: $M_\infty = 0.64$.

Results

The distributions of mean surface-pressure coefficient C_p at $M_\infty = 0.64$ are shown in Fig. 1. The distributions appear similar in shape for all of the test cases. The flows decelerate upstream of the concave corner, which is considered to be caused by the effect of displacement thickness on the effective local wall surface. Larger upstream influence region is associated with increasing concave-corner angle. Moreover, the peak pressures are observed immediately downstream of the corner followed by the expansion. Stronger upstream compression and steeper downstream expansion are associated with the increasing concave-corner angle. Further downstream, the level of mean surface-pressure coefficient tends to an equilibrium value and increases with larger concave-corner angle. At $M_\infty = 0.83$ the pressure distributions show the similar trend. The interaction region tends to expand more significantly in both upstream and downstream.

Based on the mean surface-pressure distributions, the upstream influence x_u^*, which is associated with the upstream propagation of the disturbance, can be determined as the intercept of the tangent to the maximum pressure gradient with the undisturbed surface pressure.[5] Moreover, the downstream influence x_d^* can be estimated from the corner to the intersection of the tangent through the downstream pressure data with the approximately equilibrium downstream pressure. Because the equilibrium downstream pressure can only be approximately obtained, the estimation of the downstream influence region is subjected to more uncertainty, which is estimated to be 0.3 δ_0 at $\alpha = 15$ deg. The extent of the interaction region ξ with the presence of a concave corner is then obtained in terms of the upstream and downstream influence regions ($\xi = x_u^* + x_d^*$). Figure 2a shows the upstream influence and downstream influence data. It appears that the concave-corner angle is the major parameter characterizing the upstream influence, which also increases slightly at $M_\infty = 0.83$. For the downstream influence it increases with the concave-corner angle, and the Mach-number effect is more significant.

Further, the inviscid similarity parameters ($M_\infty^2\,\alpha$ or $M_\infty\alpha$) and a similar combined similarity parameter [$\sqrt{(1 - M_\infty^2\,\alpha)}$] were examined as the scaling parameter for the upstream and downstream influences. It was found that the parameters [$M_\infty^2\,\alpha$ and $\sqrt{(1 - M_\infty^2\,\alpha)}$] appeared to not be applicable for the present test conditions. On the

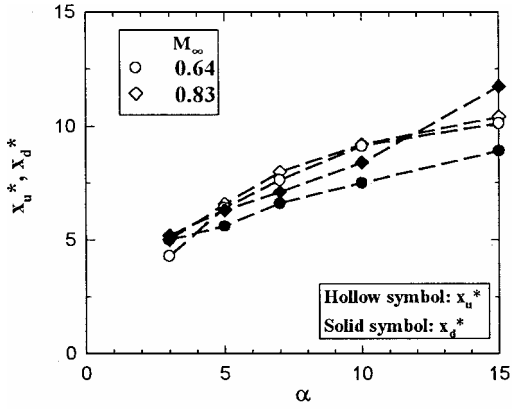

a)

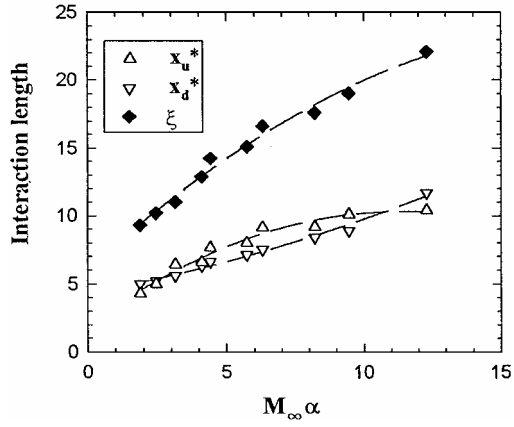

b)

Fig. 2 Interaction region.

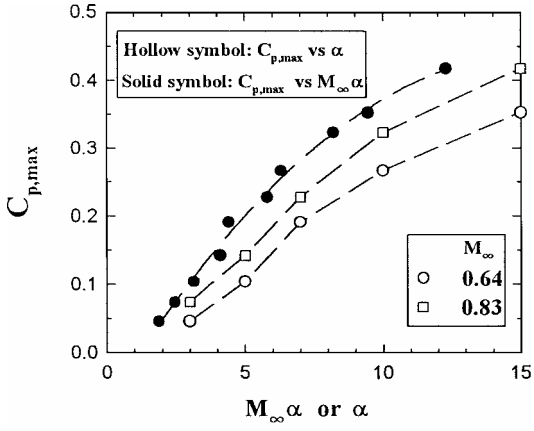

Fig. 3 Peak pressure.

other hand, the scaling parameter $M_\infty\alpha$ is more suitable (Fig. 2b). The upstream influence appears to be a quadratic function of $M_\infty\alpha$, and the correlation of the downstream influence and $M_\infty\alpha$ is also reasonably good. The extent of the interaction region shows a similar trend as the upstream and downstream influences. A good collapse of the data with $M_\infty\alpha$ can be seen.

The peak pressure downstream of the corner can be used to characterize the strength of the upstream compression processes. In Fig. 3 it can be seen that the peak pressure downstream of the concave corner can also be scaled with $M_\infty\alpha$. Stronger compression is associated with increasing freestream Mach number and concave-corner angle. Note that the peak pressure at $M_\infty\alpha = 12.30$ increases up to 42% of dynamic pressure.

Conclusions

Experiments were carried out to study the characteristics of compressible concave-corner flows. The surface-pressure distributions show similar characteristics for all of the test cases. The flows decelerate upstream of the corner and accelerate downstream of the corner. Stronger upstream compression and downstream expansion are observed with increasing Mach number and concave-corner angle, which induce a larger interaction region. The similarity parameter $M_\infty\alpha$ appears to be a suitable scaling parameter to characterize the compressible concave-corner flows, which include the interaction region (upstream and downstream influences) and the upstream compression (peak pressure).

Acknowledgments

The research was support by National Science Council (NSC 90-2212-E-006-132). The support is gratefully acknowledged. The author also thanks the technical support of the Aerospace Science and Technology Research Center/National Cheng-Kung University technical staffs with the experiments.

References

[1]Rajeswari, B., and Prabhu, K. R., "Optimum Flap Schedules and Minimum Drag Envelopes for Combat Aircraft," *Journal of Aircraft*, Vol. 24, No. 4, 1987, pp. 412–414.

[2]Bolonki, A., and Gilyard, G. B., "Estimated Benefits of Variable-Geometry Wing Camber Control for Transport Aircraft," NASA TM-1999-206586, Oct. 1999.

[3]Szodruch, J., and Hilbig, R., "Variable Wing Camber for Transport Aircraft," *Progress in Aerospace Science*, Vol. 25, No. 3, 1988, pp. 297–328.

[4]Chung, K., "Transition of Subsonic and Transonic Expansion Flows," *Journal of Aircraft*, Vol. 37, No. 6, 2000, pp. 1079–1082.

[5]Lu, F. K., "Fin Generated Shock-Wave Boundary Layer Interactions," Ph.D. Dissertation, Mechanical Engineering, Penn State Univ., PA, May 1988.

Optimum Downwash Behind Wings in Formation Flight

James W. Frazier* and Ashok Gopalarathnam†
North Carolina State University, Raleigh, North Carolina 27695

Nomenclature

b	=	aircraft wing span
C_{Di}	=	aircraft-induced drag coefficient
C_L	=	aircraft lift coefficient
C_l	=	local section lift coefficient
c	=	local chord
D	=	aircraft induced drag
$\boldsymbol{I}$	=	influence coefficient matrix of size $n \times n$
L	=	aircraft lift
n	=	number of horseshoe vortices on all of the aircraft
P, Q	=	constants used in defining downwash distribution
R	=	aircraft rolling moment
V_∞	=	freestream velocity
w	=	Trefftz-plane downwash

Received 3 October 2002; revision received 8 February 2003; accepted for publication 9 February 2003.

*Graduate Research Assistant, Department of Mechanical and Aerospace Engineering, Box 7910; currently Student Test Pilot Officer, U.S. Naval Test Pilot School, Patuxent River, MD 20670.

†Assistant Professor, Department of Mechanical and Aerospace Engineering, Box 7910; ashok_g@ncsu.edu. Member AIAA.